JACS
JOURNAL OF THE AMERICAN CHEMICAL SOCIETY
Article
pubs.acs.org/JACS

Efficient Liver Targeting by Polyvalent Display of a Compact Ligand for the Asialoglycoprotein Receptor

Carlos A. Sanhueza,[†,‡] Michael M. Baksh,[†,‡] Benjamin Thuma,[§] Marc D. Roy,[∥] Sanjay Dutta,[‡] Cathy Préville,[§] Boris A. Chrunyk,[§] Kevin Beaumont,[⊥] Robert Dullea,[#] Mark Ammirati,[§] Shenping Liu,[§] David Gebhard,[§] James E. Finley,[∥] Christopher T. Salatto,[#] Amanda King-Ahmad,[§] Ingrid Stock,[§] Karen Atkinson,[§] Benjamin Reidich,[#] Wen Lin,[§] Rajesh Kumar,[▽] Meihua Tu,[⊥] Elnaz Menhaji-Klotz,[⊥] David A. Price,[⊥] Spiros Liras,[⊥] M. G. Finn,*[,†,‡] and Vincent Mascitti*[,§]

[†]School of Chemistry & Biochemistry, Georgia Institute of Technology, 901 Atlantic Avenue, Atlanta, Georgia 30332, United States
[‡]Department of Chemistry and The Skaggs Institute for Chemical Biology, The Scripps Research Institute, 10550 N. Torrey Pines Road, La Jolla, California 92037, United States
[§]Pfizer Medicine Design, Eastern Point Road, Groton, Connecticut 06340, United States
[∥]Pfizer Drug Safety R&D, Eastern Point Road, Groton, Connecticut 06340, United States
[⊥]Pfizer Medicine Design, Main Street, Cambridge, Massachusetts 02139, United States
[#]Pfizer CVMET Biology, Main Street, Cambridge, Massachusetts 02139, United States
[▽]Pfizer Medicinal Sciences, Eastern Point Road, Groton, Connecticut 06340, United States

Supporting Information

ABSTRACT: A compact and stable bicyclic bridged ketal was developed as a ligand for the asialoglycoprotein receptor (ASGPR). This compound showed excellent ligand efficiency, and the molecular details of binding were revealed by the first X-ray crystal structures of ligand-bound ASGPR. This analogue was used to make potent di- and trivalent binders of ASGPR. Extensive characterization of the function of these compounds showed rapid ASGPR-dependent cellular uptake in vitro and high levels of liver/plasma selectivity in vivo. Assessment of the biodistribution in rodents of a prototypical Alexa647-labeled trivalent conjugate showed selective hepatocyte targeting with no detectable distribution in nonparenchymal cells. This molecule also exhibited increased ASGPR-directed hepatocellular uptake and prolonged retention compared to a similar GalNAc derived trimer conjugate. Selective release in the liver of a passively permeable small-molecule cargo was achieved by retro-Diels–Alder cleavage of an oxanorbornadiene linkage, presumably upon encountering intracellular thiol. Therefore, the multicomponent construct described here represents a highly efficient delivery vehicle to hepatocytes.

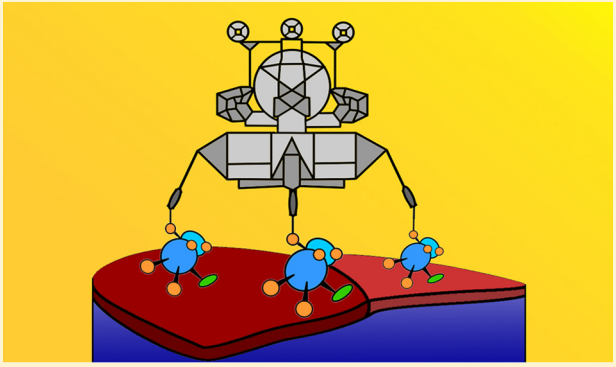

INTRODUCTION: AN OPTIMIZED ASGPR LIGAND MOTIF

By virtue of its extraordinary rates of transport, the asialoglycoprotein receptor (ASGPR) is an attractive target for the importation of diagnostic and therapeutic molecules into hepatocytes.[1−3] However, monosaccharide ligands of the ASGPR usually bind with low affinity (K_d in the high μM to low mM range),[4] and so multimerization of these species is used to achieve levels of affinity thought to be required for the delivery of therapeutic cargos.[5−9] To our knowledge, the relationship of high-affinity binding to transport (that is, to binding, membrane translocation, and release) has not been extensively explored.

We previously described several series of ASGPR ligands based on substituent variations at the anomeric, 2-, 5-, and 6-positions of the galactosamine (GalNAc) skeleton.[10] This work, along with previous studies of Ernst and co-workers[4,11] and others,[12] shows that substantial variations can be tolerated as long as the C3−C4 diol is presented in the proper orientation for interaction with a proximal calcium ion of the receptor.[13] Although it is possible to access analogues of improved affinity in this way, such compounds often suffer from a dramatic decrease in ligand efficiency (LE),[14−17] as shown for examples **1**−**3** in Figure 1. In combination with their multistep and low-

Received: December 21, 2016
Published: February 23, 2017

DOI: 10.1021/jacs.6b12964
J. Am. Chem. Soc. 2017, 139, 3528−3536

yielding synthesis, this makes them suboptimal alternatives as ASGPR-targeting ligands.

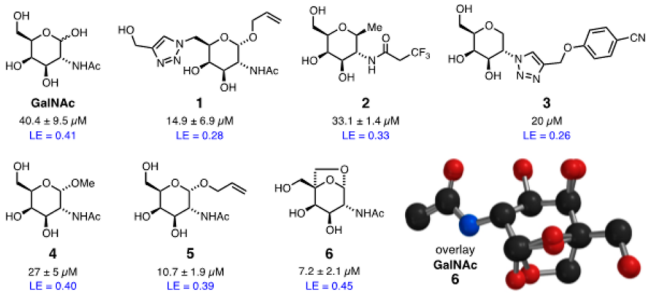

Figure 1. ASGPR ligands with ($1/K_{ads}$) values for immobilized ASGPR measured by surface plasmon resonance, plus calculated ligand efficiency (LE) values. (Bottom right) Overlay of the calculated minimum-energy conformations of GalNAc and compound **6**, showing close overlap of the pyranose rings and substituents between the two structures. Values for **1**, **2**, and **5** are from ref 10; compound **3** is found in ref 4.

Examination of the published X-ray crystal structure of ASGPR binding domain (PDB: 1dv8)[25] led us to postulate that one could potentially optimize the interaction between the hydrophobic α-face of the pyranose and the tryptophan residue Trp 243.[18] In order to improve both affinity and LE, we reasoned that a bridged ketal structure such as **6** should lock in a conformation in which the α-face is accessible and the 6-hydroxymethyl and 2-*N*-acetyl groups retain their positions (Figure 1). Molecular mechanics calculations showed the lowest-energy conformation of **6** to match that of GalNAc, but with ~1.6 kcal/mol separating it from the next-higher-energy structure. In contrast, five distinct low-energy conformations of GalNAc are within 0.5 kcal/mol of each other, suggesting that **6** should exhibit a much greater occupancy of the favored ASGPR-binding conformation than GalNAc. This is purchased at the cost of the addition of only a single extra methylene group compared to GalNAc, thereby potentially leading to an increase in LE. Similar bridged ketal ring systems were reported during the development of the antidiabetes medication ertugliflozin.[19,20]

Compound **6** was initially prepared in relatively low overall yield as shown in Figure 2A. Treatment of commercially available methyl-α-D-2-acetamido-2-deoxygalactopyranoside **4** in the presence of galactose oxidase and catalase in a phosphate buffer produced the corresponding intermediate aldehyde,[21]

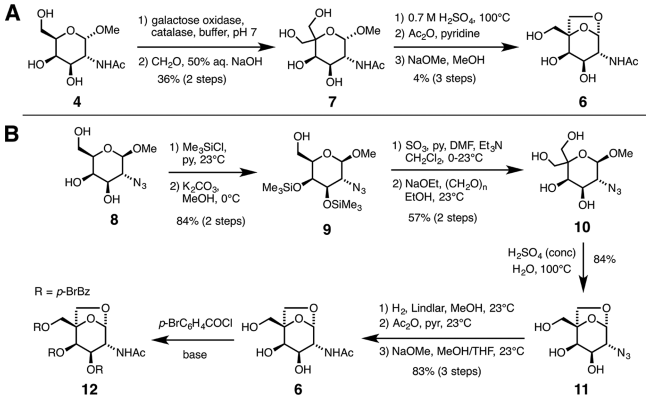

Figure 2. Initial (A) and improved (B) synthetic routes to **6**.

which was subjected without purification to aldol-Cannizzaro conditions to give polyol intermediate **7** in 36% yield over two steps.[22] Acid-promoted bridged ketal formation followed by peracetylation and saponification gave the desired product in sufficient quantities for measurement of binding to immobilized ASGPR by surface plasmon resonance (SPR) as described earlier.[10] These measurements provide Langmuir adsorption coefficients (K_{ads}), the reciprocals of which represent experimental approximations of dissociation constants.[23] Compound **6** exhibited almost 6-fold better affinity than GalNAc ($1/K_{ads}$ = 7.2 vs 40 μM), giving a calculated ligand efficiency (0.45) greater than that of the natural ligand (0.41).

The synthetic route shown in Figure 2B was developed to allow access to multigram quantities of this lead structure and derivatives for further in vitro and in vivo profiling. Persylilation of azide **8**[24] followed by base-promoted regioselective deprotection of the primary hydroxyl group gave **9**. Sequential Parikh–Doering oxidation and aldol-Cannizzaro reactions cleanly installed the desired tetrasubstituted carbon at C-5 (compound **10**). Stereoselective bridged ketal formation under acidic conditions gave **11** in good yield. Finally, azide reduction followed by peracetylation/saponification provided **6** as a white solid. This route provided access to **6** in 8 steps and 33% overall yield, as well as to other derivatives. Single-crystal X-ray diffraction analysis of derivative **12** was used to confirm the bridged ketal structure of **6** (Supporting Information).

SPR measurements of ASGPR binding (Figure 3) confirmed the importance of both the *N*-acetyl group (compound **13** vs **6**)

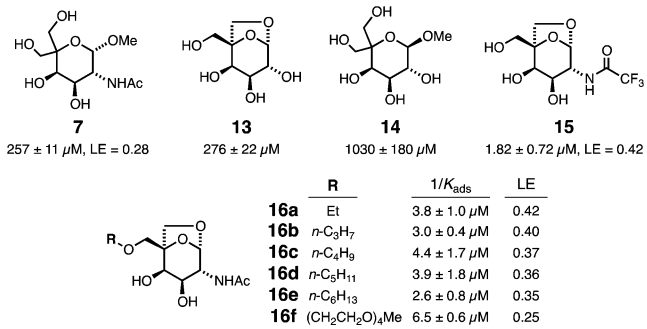

	R	$1/K_{ads}$	LE
16a	Et	3.8 ± 1.0 μM	0.42
16b	*n*-C_3H_7	3.0 ± 0.4 μM	0.40
16c	*n*-C_4H_9	4.4 ± 1.7 μM	0.37
16d	*n*-C_5H_{11}	3.9 ± 1.8 μM	0.36
16e	*n*-C_6H_{13}	2.6 ± 0.8 μM	0.35
16f	$(CH_2CH_2O)_4Me$	6.5 ± 0.6 μM	0.25

Figure 3. ASGPR ligands discussed in the text with $1/K_{ads}$ values for ASGPR determined by surface plasmon resonance.

and the bicyclic nature of the core structure (**7** vs **6** and **14** vs **13**). We had previously established for other GalNAc analogues that a trifluoroacetamide unit at C2 improved binding by 3–10-fold relative to acetamide,[10] and this trend was also observed here (compound **15** vs **6**). (Compound **6** was used for the in vivo studies described below because of uncertainty associated with the long-term metabolic stability of the trifluoroacetamide group.) Alkylation of the C6-hydroxyl was envisioned as a way to attach this motif to cargo molecules, and alkyl and oligo(glycol) ethers **16a–f** derived from **6** retained full affinity for the receptor.

Atomic Resolution Structure of ASGPR–Ligand Complexes. Although the crystals used for the reported structure of the ASGPR carbohydrate-binding H1 domain (PDB: 1dv8) were grown in the presence of 20 mM lactose, the sugar does not appear in the structure.[25] Therefore, we and others have relied on docking calculations, which show that the GalNAc-binding region is shallow and a difficult target for high-affinity monomeric ligands,[26] a conclusion reinforced by

DOI: 10.1021/jacs.6b12964
J. Am. Chem. Soc. 2017, 139, 3528–3536

structures of GalNAc bound to homologous mannose receptor derivatives (PDB: 1bch, 1bcj, 1fif, and 1fih).[27,28] We were able to secure more direct structural information by crystallizing the ASGPR carbohydrate-binding domain with lactose and with compound **6**, and obtaining diffraction data with well-resolved ligand densities. The resulting structures are shown in Figure 4.

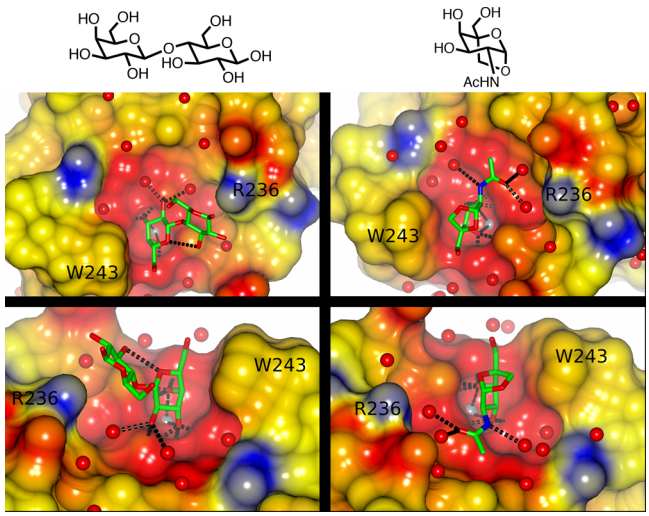

Figure 4. X-ray crystal structures of the ASGPR carbohydrate-binding domain with (left) lactose (PDB: 5JPV) and (right) compound **6** (PDB: 5JQ1). The top panels show the shallow binding pocket from above; the bottom panels show a side view highlighting hydrophobic interactions with Trp 243 and interactions with the acetamide group of **6** along the bottom of the pocket. Red = negative surface charge, blue = positive surface charge, and yellow = hydrophobic surface. Hydrogen bonds and bonds to metal ion (gray sphere) are shown in dashes. Small red spheres represent bound water molecules identified crystallographically.

These structures provide the first high-resolution look at the ASGPR–galactose-binding interaction. The sugar-binding mode was found to be consistent with previous analogue structures and predictions, showing interactions of the hydroxyls at C-3 and C-4 of the β-D-galactose ring with the required calcium ion.

Comparisons of affinity and LE of **6** versus its uncyclized precursors **4** and **7** support the hypothesis of a productive van der Waals interaction with Trp 243. Such an interaction is apparent in both structures, with ASGPR·**6** exhibiting a more extensive pyranose–indole overlap at a measured distance of 4 Å (Figure 4). The acetamide group of **6** conforms nicely to the channel floor (defined by Tyr 272, His256, Asn264, and Asp266 residues), whereas the 6-hydroxymethyl substituent extends away from the protein, allowing for cargo attachment. The structural details of the binding of other ligands reported previously, which have substituents at various places around the *N*-acetylgalactose core,[10] will be discussed elsewhere.

MULTIVALENT LIGANDS

The use of galactosyl-based ligands for the targeting of liver cells where ASGPR expression is highest has relied for many years on the creation of multivalent molecules to enhance receptor binding beyond the low-micromolar level,[29−32] with recent reports of targeted siRNA and antisense DNA delivery being especially exciting.[33−35] Multimerization of the bicyclic ASGPR-binding motif was accomplished by a convergent design relying on azide–alkyne cycloaddition to connect an azide-terminated version of ligand **6** to propargylic ethers of mono-, di-, and trivalent ethanolamines (Figure 5). The amino

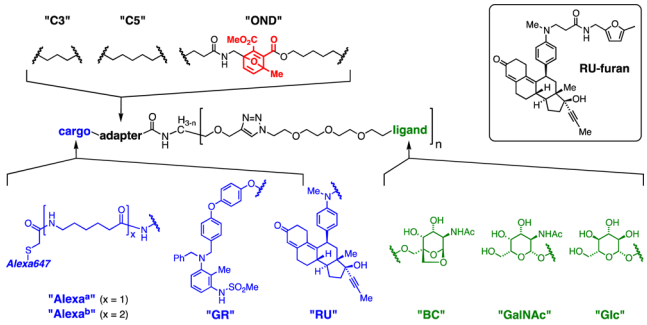

Figure 5. Modular composition of the multivalent compounds discussed in the text.

group was used to connect to the carboxylic acid derivatives of candidate "cargo" molecules: a fluorescent probe (Alexa-Fluor647, with two different linker lengths, designated "Alexa^a" and "Alexa^b") and two model drug-like compounds, a nonsteroidal glucocorticoid receptor modulator (designated "GR"),[36] and the steroidal glucocorticoid antagonist RU-486 (mifepristone, designated "RU"). Analogous compounds bearing the natural GalNAc and glucose (Glc) ligands in place of the bicyclic derivative were prepared by the same modular approach.

With the expectation that drug release from ASGPR-targeting motifs would be necessary, we also prepared variants incorporating the thiol-sensitive oxanorbornadiene (OND)[37,38] linker by the route shown in the Supporting Information. This system relies on a two-step Michael addition/retro-Diels–Alder sequence that is programmed to occur rapidly in the presence of intracellular levels of reduced thiols such as glutathione. Thus, the various molecules explored here are referred to in the form "cargo-adapter-ligand", as in "**GR-C3-(BC)$_2$**" for a compound bearing two bicyclic bridged ketal ASGPR ligands, connected to a GR cargo by a simple propyl (C_3) chain. The labeling scheme is shown in Table 1. Not all of the possible combinations of ligand, cargo, and valence were explored.

Table 1. Binding and Activity Results for Selected Compounds

compound	$1/K_{ads}$	compound	$1/K_{ads}$
Alexa^a-C3-(BC)$_1$	4.1 μM	**Gr-C3-(BC)$_1$**	nonspecific
Alexa^a-C3-(BC)$_2$	0.96 ± 0.01 nM	**Gr-C3-(BC)$_2$**	0.49 ± 0.01 nM
Alexa^a-C3-(BC)$_3$	30 ± 5 pM	**Gr-C3-(BC)$_3$**	71 ± 30 pM
Ru-C3-(BC)$_2$	1.48 ± 0.05 nM		

The ASGPR-binding ability of a subset of multivalent conjugates was measured by surface plasmon resonance (SPR), with results summarized in Table 1. The monovalent conjugate **Alexa^a-C3-(BC)$_1$** bound with low micromolar affinity, consistent with values for the parent bicyclic **6** and analogues shown in Figure 3 (**15**, **16a–f**). The corresponding GR modulator adduct, **GR-C3-(BC)$_1$**, exhibited competing nonspecific interactions in the SPR assay, perhaps to be expected given the hydrophobic nature of the cargo. Bivalent structures **Alexa^a-C3-(BC)$_2$**, **GR-C3-(BC)$_2$**, and **RU-C3-(BC)$_2$** all showed ∼1000-fold improvement in avidity (binding

DOI: 10.1021/jacs.6b12964
J. Am. Chem. Soc. 2017, 139, 3528–3536

constants approximately 1 nM), and the trivalent analogues (**Alexa^a-C3-(BC)$_3$** and **GR-C3-(BC)$_3$**) showed a further 7−30-fold improvement to the midpicomolar range. After binding to immobilized ASGPR on the SPR chip at pH 7.4, **Alexa^a-C3-(BC)$_3$** was rapidly released upon exposure to buffer at pH 5.2 or 5.7; whereas at pH 6.5, much less release was observed (Figure S3). This is consistent with the reported pH dependence of ASGPR binding to monomeric natural ligands.[39,40]

ASGPR Engagement In Vitro. The ability of representative conjugates to engage the ASGPR was assessed by fluorescence microscopy in cultured HepG2 and SK-Hep cells. These cell lines have some of the properties of hepatocytes and are standard in vitro models; while both exhibit lower levels of asialoglycoprotein receptor compared to primary hepatocytes, the HepG2 line expresses a much higher density of ASGPR on the cell surface than SK-Hep cells. This was verified prior to use by antibody staining (Figure S4). Cargo uptake by HepG2 cells was found to be extensive for di- and trivalent AlexaFluor conjugates of the bicyclic motif **6**, but much less pronounced with the monovalent analogue (Figures S8 and S10). Dye-labeled asialoorosomucoid (ASOR), commonly used as a positive control for ASGPR-mediated endocytosis, was taken into HepG2 cells better than the monovalent **Alexa^a-C3-(BC)$_1$** compound, but to a significantly lesser degree than the di- and trivalent analogues. Little or no uptake into HepG2 cells was observed for the analogous glucosyl derivatives (Figure S5), and SK-Hep cells were very poorly targeted by any of these compounds (Figure S9). These results were confirmed by quantitative flow cytometry (Figure 6, which of course measures total internalized signal, both

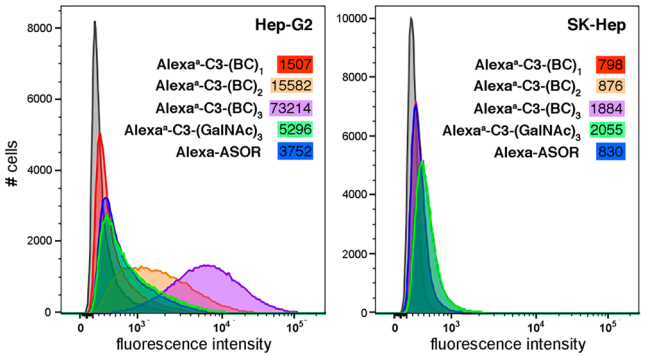

Figure 6. Flow cytometry analysis of the indicated cells treated with the indicated molecules (100 nM, 30 min, room temperature). Numerical values are the average number of dye-labeled molecules taken up per cell, derived from comparison to standardized samples.

cytosolic and endolysosomal), revealing a 10-fold increase in uptake of dye-labeled **Alexa^a-C3-(BC)$_3$** versus **Alexa^a-C3-(GalNAc)$_3$** by ASGPR-rich cells.

As shown in the Supporting Information, dye-labeled **Alexa^a-C3-(BC)$_n$** conjugates internalized into HepG2 cells appeared to be both colocalized with endosomes and in the cytosol. Furthermore, uptake of these compounds was found to be blocked in the presence of a low concentration of chlorpromazine, known to inhibit clathrin-mediated endocytosis,[41] as expected.[42,43]

ASGPR ligand valency also had a strong effect on the rate of receptor-mediated cellular uptake. Figure 7A shows marked differences for HepG2 cells in the presence of 100 nM solutions

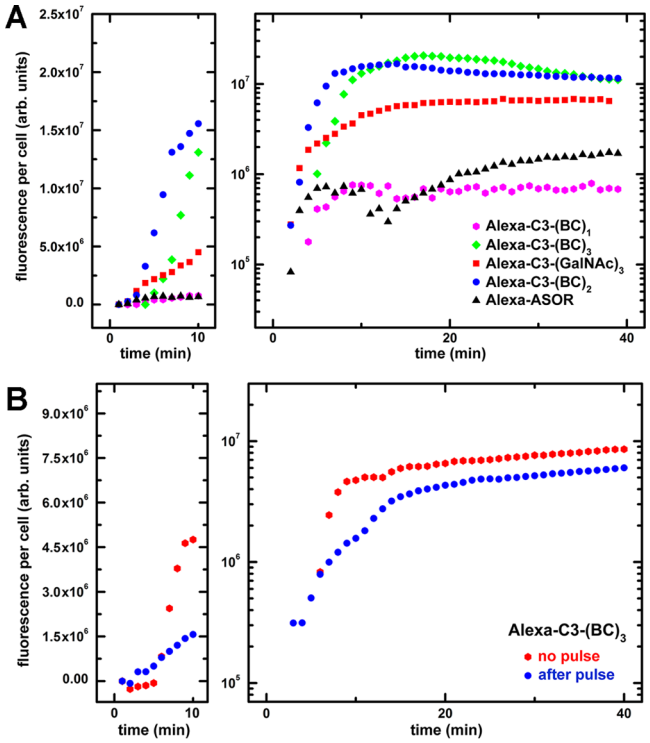

Figure 7. (A) Mean fluorescence intensity (MFI) per cell, measured by fluorescence microscopy, for HepG2 cells treated with 100 nM of the indicated molecule. (B) Pulse-chase experiment in which HepG2 cells were treated with 100 nM of a tripodal ligand lacking a cargo [**(BC)$_3$-NH$_2$**] for 30 min, washed three times, and then treated with 100 nM of the dye-labeled trimer (starting at time = 0). For comparison, uptake curves for the dye-labeled compounds alone (100 nM) are shown in red ("no pulse"). The first 10 min of the experiment is shown on the left on a linear fluorescence intensity scale; on the right is the full experiment on a logarithmic scale. Analogous results with other chase compounds are shown in Figure S11.

of dye−cargo conjugates, in the order BC dimer ≈ BC trimer > GalNAc trimer > ASOR ≈ BC monomer. To further probe effects on receptor recycling, a series of pulse-chase experiments was performed in which HepG2 cells were saturated with an unlabeled trivalent BC conjugate **(BC)$_3$-NH$_2$** (Supporting Information), followed by treatment with Alexa-labeled variants (100 nM), and uptake kinetics were compared to the direct treatments of dye-labeled compounds described earlier. Figure 7B shows an example in which the chase compound is **Alexa^a-C3-(BC)$_3$**. In this and analogous experiments (Figure S11), pretreatment with trivalent BC ligand induced a modest delay in follow-on internalization but no significant change in overall uptake, showing that this high-affinity molecule has a slightly delayed off-rate but does not abrogate receptor function. Similar results were observed when chasing with Alexa-labeled ASOR and **Alexa^a-C3-(GalNAc)$_3$**. These observations are consistent with the assumption that internalization rates and behavior of the di- and trivalent BC conjugates generally resemble that of the natural high-valent and high-affinity asialoorosomucoid ligand,[44] with higher affinity bestowed by the optimized nature of the bicyclic ligand.

To further explore the relative activity and potential translational impact of the compact bicyclic ligand versus GalNAc, human primary hepatocytes were treated with the triantennary versions of each, conjugated to AlexaFluor647. Figure 8 shows representative fluorescence microscopy images

DOI: 10.1021/jacs.6b12964
J. Am. Chem. Soc. 2017, 139, 3528−3536

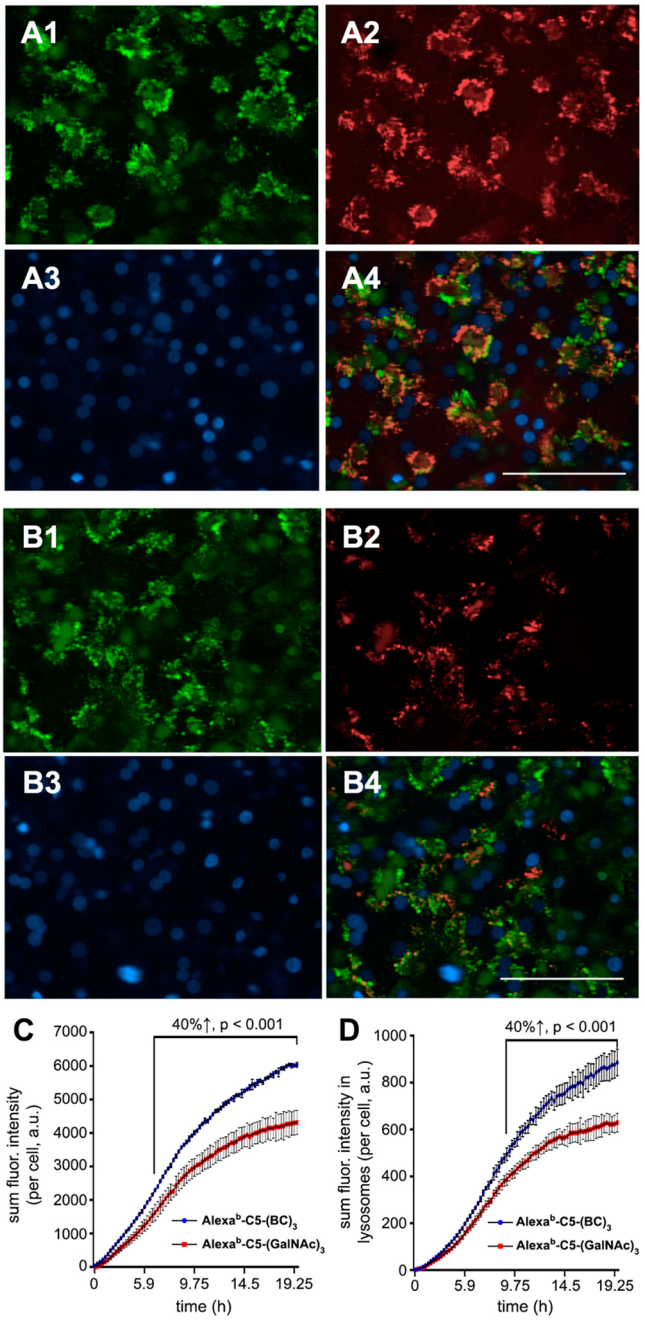

Figure 8. Human primary hepatocytes treated with (A) **Alexa^b-C5-(BC)$_3$** or (B) **Alexa^b-C5-(GalNac)$_3$** for 20 h at 1 μM. Staining: 1 = endolysosomal (pHrodo dextran); 2 = AlexaFluor647 (ASGPR-targeted compounds); 3 = nuclear (DAPI); 4 = composite overlaid images. Scale bar =100 μm. Wider-field images are shown in Figure S14. Quantification of intracellular (C) and lysosomal (D) accumulation. In each case, a statistically significant increase (~40%) was observed for the tripodal **BC** ligand vs the analogous **GalNAc** ligand.

after prolonged exposure, demonstrating more efficient uptake of the BC analogue and strong endolysosomal colocalization for both compounds. It should be noted that these dye-labeled compounds were derived from a commercial Alexa-thiol reagent, with two different connector lengths employed during the course of these studies, designated Alexa^a and Alexa^b and defined in Figure 5. No differences were noted in the behavior of conjugates having connectors of different lengths.

Liver Targeting. The glucocorticoid receptor modulator RU-486 was chosen as a model drug to illustrate the liver-targeting potential of these novel ASGPR ligands. Indeed, hepatoselective delivery of such modulators could be desirable for Type 2 diabetes treatment while minimizing risks of side effects associated with exposure of such compounds in peripheral tissues. We determined the liver/plasma ratios for various RU-486 conjugates in rats under steady-state intravenous infusion. Under these conditions, a molecule with high passive permeability (like RU-486 or RU-furan) should achieve a 1:1 unbound plasma to unbound liver concentration ratio, so long as there is no active uptake into or efflux from the liver. An unbound liver/plasma ratio greater than 1 reflects active uptake of that compound.

All compounds (except the hydrophobic **RU-furan**)[45] were formulated in 0.9% saline at 0.2 mg/mL and constantly infused into 4 male Wistar-Han rats at a rate of 10 $\mu g \cdot min^{-1} \cdot kg^{-1}$ over 7 h (total dose = 4.2 mg/kg, 21 mL/kg total volume). During this time, blood samples were taken at 0.1, 0.25, 0.5, 1, 2, 4, and 7 h following the start of the infusion, and compound concentrations were measured in the derived plasma. Steady-state values (reached within 1 h and maintained over the full 7 h in each case) are shown in Table 2; representative runs are shown

Table 2. In Vivo Results for the Distribution of Certain Adducts of RU-486 with Mono- and Multivalent ASGPR Ligand-Targeting Agents

	RU-C3-(BC)$_1$	RU-C3-(BC)$_2$	RU-C3-(BC)$_3$	RU-C3-(GalNac)$_2$	RU-C3-(GalNac)$_3$
fraction unbound, liver	0.089	0.11	0.065	0.079	0.22
fraction unbound, plasma	0.265	0.27	0.283	0.298	0.55
unbound liver:plasma ratio	0.39	9	144	0.87	8.7
	RU-C3-(Glc)$_2$	**RU-C3-(Glc)$_3$**	**RU-OND-(BC)$_2$[a]**	**RU-OND-(BC)$_3$[a]**	**RU-OND-(Glc)$_2$[a]**
fraction unbound, liver	0.13	0.12	nd[b]	nd[b]	nd[b]
fraction unbound, plasma	0.49	0.68	nd[b]	nd[b]	nd[b]
unbound liver:plasma ratio	0.22	0.02	93[c]	41[c]	0.9[c]

[a]OND = cleavable oxanorbornadiene linker (see Figure 5) releasing **RU-furan** (as shown in Figure 10). [b]Not determined due to decomposition. [c]Liver/plasma ratio determined for released **RU-furan**.

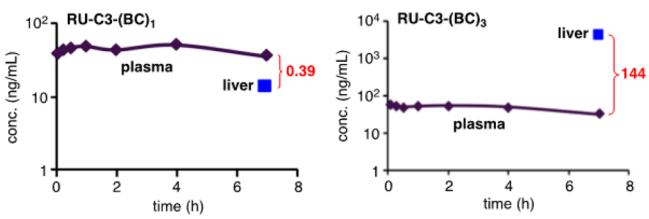

Figure 9. Representative intravenous infusion results in rat showing concentrations of free (unbound) plasma concentrations of the indicated compounds and the endpoint concentration in liver.

DOI: 10.1021/jacs.6b12964
J. Am. Chem. Soc. 2017, 139, 3528−3536

in Figure 9. After 7 h of infusion, each animal was sacrificed, the liver was removed, and the compound concentration was determined in that organ. In addition to these values of total plasma and liver concentrations, in vitro equilibrium dialysis was used to determine the binding of these compounds in these environments (Table 2), as only unbound compound is available to exert a pharmacological effect. See Supporting Information for detailed procedures and analytical methods.

In general, all of the compounds tested showed higher binding (lower fraction unbound) in liver homogenate than in plasma. The aforementioned measurements of ASGPR-binding avidity and in vitro cell uptake proved to be predictive of the observed liver/plasma ratio, with increasing valency showing dramatic enhancements in each case (Figure 9 and Table 2). Thus, the noncleavable series [**RU-C3-(BC)$_n$**] showed values of 0.4, 9, and 144 for monomer, dimer, and trimer conjugates, respectively, with the last value representing an unusually high figure. The same trend, but lower absolute values, was observed for the weaker-binding GalNAc ligand (0.87 vs 8.7 for dimer vs trimer). The liver/plasma ratios for the glucosyl conjugates were <1.0, consistent with the expected poor permeability and lack of receptor-mediated uptake of these compounds. Further analysis of the significance of the differences in liver/plasma ratios for **BC** and **GalNAc** conjugates (which rely on detection of the parent compounds by mass spectrometry) would require a complete assessment of their metabolism, which may differ.

The cleavable ASGPR-binding OND conjugate was also effective in delivering small-molecule cargo to hepatocytes (Figure 10 and Table 2). OND linkers undergo facile Michael

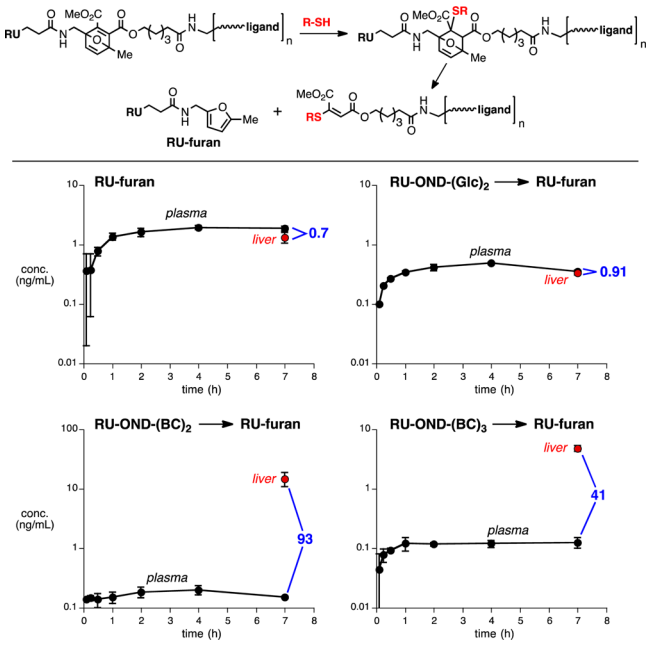

Figure 10. (Top) Thiol-triggered release of **RU-furan** cargo. (Bottom) Delivery of **RU-furan** by steady-state infusion of the indicated conjugates. Values in blue represent the free liver/plasma ratio at 7 h.

addition by free thiol compounds, inducing subsequent retro-Diels–Alder fragmentation of the resulting adducts.[37,38] The bivalent and trivalent OND conjugates **RU-OND-(BC)$_2$** and **RU-OND-(BC)$_3$** partitioned nicely into liver and released their cargo **RU-furan** with high liver/plasma ratios of 93 and 41, respectively. **RU-furan** alone showed no such selectivity (liver/plasma ratio = 0.7) as would be expected from a freely permeable small molecule. While **RU-OND-(BC)$_n$** compounds can react in principle with serum albumin or undergo ester hydrolysis,[46] these molecules showed good serum and plasma stability (Supporting Information). The majority of **RU-furan** release therefore presumably occurs after cellular internalization via ASGPR-mediated uptake and exposure to intracellular thiol (principally glutathione).

Hepatic Distribution. To further characterize the liver-targeting function of these molecules and compare both GalNAc- and BC-derived conjugates for hepatoselective delivery of therapeutic modalities, we conducted an in vivo biodistribution study in C57BL/6N mice using prototypical Alexa647-labeled conjugates **Alexa^b-C5-(BC)$_3$** and **Alexa^b-C5-(GalNAc)$_3$**. Both tripodal variants were shown to achieve similar systemic exposure at an early time point (15 min after tail vein injection) and then were rapidly cleared (Supporting Information).[47] The hepatic exposure and cellular distribution of these compounds were evaluated at 1, 2, and 4 h postdose using confocal microscopy. Representative images at each time point are shown in Figure 11 and visually demonstrate the elevated liver accumulation of **Alexa^b-C5-(BC)$_3$** relative to **Alexa^b-C5-(GalNAc)$_3$** at each time point. This was confirmed by image analysis quantification of liver exposure, showing 8–350 fold increase in the percentage of liver tissue area positive for the dye (Figure 11H). In addition, liver tissue area positive

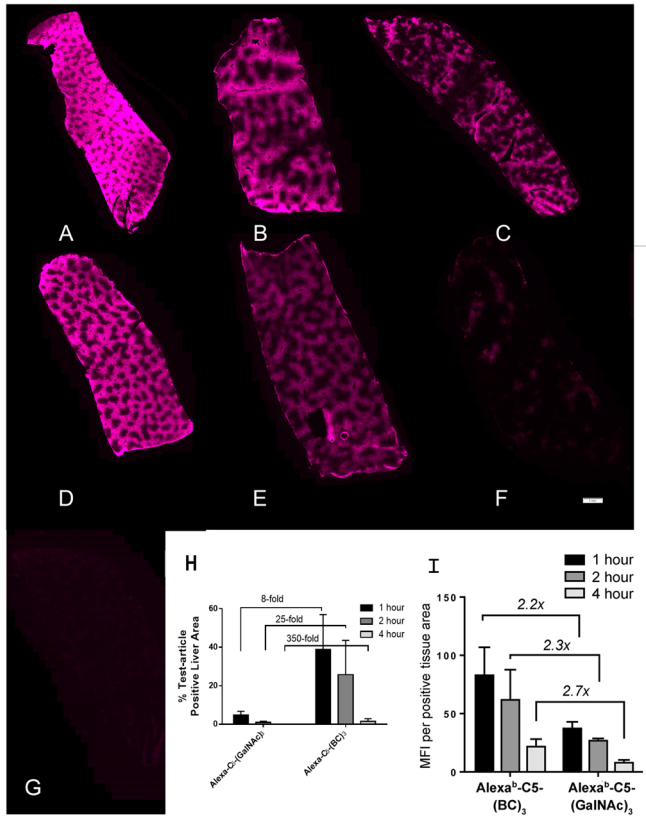

Figure 11. Whole tissue scans of mouse livers treated with (A–C) **Alexa^b-C5-(BC)$_3$** for 1, 2, and 4 h, respectively; (D–F) **Alexa^b-C5-(GalNAc)$_3$** for 1, 2, and 4 h, respectively; (G) vehicle only. Scale bar = 1 mm. Compound exposure in liver sections quantified by fluorescence microscopy: (H) percent of liver tissue area positive for dye and (I) mean fluorescence intensity of dye-positive tissue area representing relative exposure levels.

DOI: 10.1021/jacs.6b12964
J. Am. Chem. Soc. 2017, 139, 3528–3536

for **Alexa^b-C5-(BC)$_3$** had, on average, ~2−3-fold greater mean fluorescence intensity (MFI) compared to **Alexa^b-C5-(GalNAc)$_3$** positive tissue area (Figure 11I). All other tissues evaluated were negative for **Alexa^b-C5-(GalNAc)$_3$** and **Alexa^b-C5-(BC)$_3$** exposure.

Characterization of both **Alexa^b-C5-(GalNAc)$_3$** and **Alexa^b-C5-(BC)$_3$** distribution within the liver (Figure 12) revealed

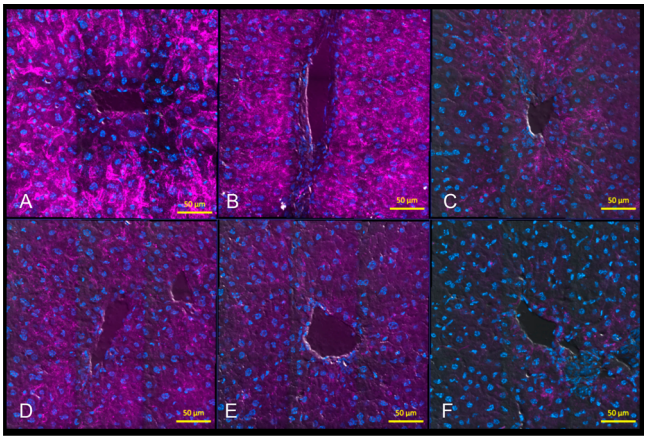

Figure 12. High-magnification composite images of perivenous regions of liver, from mice dosed with **Alexa^b-C5-(BC)$_3$** (panels A−C = 1, 2, 4 h) or **Alexa^b-C5-(GalNAc)$_3$** (panels D−F = 1, 2, 4 h). Purple color is fluorescence of the dosed compound, while nuclei are stained blue (scale bars = 50 μm).

centrilobular accumulation, correlating with reported ASPGR expression across the hepatic lobule in rodents.[48] These observations further support a receptor-mediated mechanism of cellular uptake within the liver. To further evaluate the cellular distribution of the tripodal ligands, high-resolution images were captured using confocal microscopy. Figure 13B shows the greater level of **Alexa^b-C5-(BC)$_3$** accumulation within the cytoplasm of liver cells compared to **Alexa^b-C5-(GalNAc)$_3$** at 4 h (Figure 13A). **Alexa^b-C5-(BC)$_3$** accumulation was associated with cytoplasmic puncta within hepatocytes (Figure 13C) that are not present in nonparenchymal cells. Intracellular accumulation of both ASGPR ligands within nonparenchymal cell types was not obvious.

Alexa^b-C5-(GalNAc)$_3$ and **Alexa^b-C5-(BC)$_3$** accumulation in hepatocytes was also measured by flow cytometry at 4 h. On average, hepatocytes isolated from mice treated with **Alexa^b-C5-(BC)$_3$** had an 8-fold greater positive population compared to hepatocytes isolated from **Alexa^b-C5-(GalNAc)$_3$** treated mice (Figure 14A). In addition, hepatocytes positive for **Alexa^b-C5-(BC)$_3$** had, on average, ~40% greater mean fluorescence intensity (MFI) compared to **Alexa^b-C5-(GalNAc)$_3$** positive hepatocytes (Figure 14B), confirming elevated intrahepatocellular levels of **Alexa^b-C5-(BC)$_3$** at this time point. This latter observation also correlates nicely with in vitro uptake results obtained with human primary hepatocytes (Figure 8).

■ CONCLUSIONS

Consideration of the likely intermolecular interactions that allow ASGPR to recognize *N*-acetylgalactosamine residues led to the design and synthesis of a bicyclic compound (**6**, or "**BC**") with superior ligand efficiency and binding affinity. The first reported X-ray crystal structures of ligand-bound ASGPR

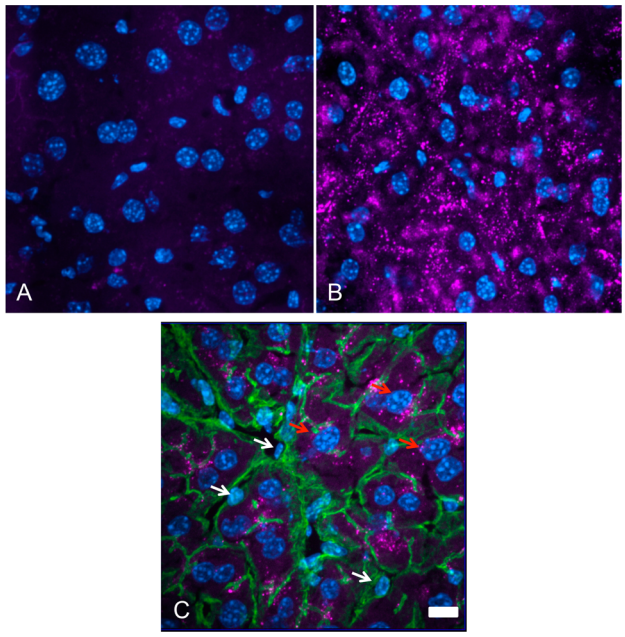

Figure 13. High-magnification images of cellular liver distribution, 4 h after dosing, demonstrating more efficient uptake of the construct based on bicyclic ligand **6**. (A) **Alexa^b-C5-(GalNAc)$_3$** and (B, C) **Alexa^b-C5-(BC)$_3$**. In panel C, the fluorescent compound is associated with hepatocytes (red arrows), while accumulation in nonparenchymal cells (white arrows) is not apparent (scale bar = 10 μm). Purple = dosed compound (AlexaFluor 647); blue = nuclei (DAPI); and green = actin (AlexaFluor 488).

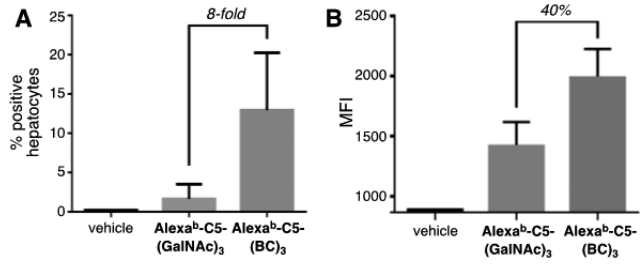

Figure 14. (A, B) Hepatic exposure of trivalent compounds quantified by flow cytometry. (A) Percent of isolated hepatocytes positive for each dosed compound. At 4 h, animals dosed with **Alexa^b-C5-(BC)$_3$** had 8-fold greater population of positive hepatocytes, compared to animals dosed with **Alexa^b-C5-(GalNAc)$_3$**. (B) Mean fluorescence intensity (MFI) of the indicated compound in hepatocytes positive for Alexa647 dye at 4 h. At this time point, hepatocytes positive for **Alexa^b-C5-(BC)$_3$** had 40% greater intracellular levels compared to positive hepatocytes from animals dosed with **Alexa^b-C5-(GalNAc)$_3$**.

were obtained, validating these predictions and the models used by others.

A modular synthetic approach enabled the synthesis of mono-, di-, and trivalent versions of this ligand (and of comparison GalNAc and glucose moieties), each carrying a single copy of a "cargo" compound. The performance of these molecules in binding ASGPR, mediating internalization into cultured cell lines and primary cells, and mediating trafficking and targeting in vivo was assessed by a variety of techniques. A consistent relationship was observed, with ASGPR avidity correlating with all the functional assays, with the bicyclic structure superior to GalNAc in the rate and extent of cellular uptake in vitro. This cellular uptake was dominated by ASGPR, and trivalent structures involving the bicyclic ligand were

DOI: 10.1021/jacs.6b12964
J. Am. Chem. Soc. 2017, 139, 3528−3536

usually found to exceed the reported outstanding affinity and uptake exhibited by the natural asialoorosomucoid ligand while retaining the natural ligand's ability to allow for rapid receptor recycling.

As has been previously observed,[29] multimerization of ASGPR ligands (usually GalNAc) is a potent strategy for enhancement of binding to hepatocytes in vitro[5−8,49,50] and for delivery to the liver.[32−34,51−53] Because multiantennary displays of galactosyl ligands are effective agents in binding a number of different cell types,[54,55] it was important to verify[56,57] that, indeed, a prototypical trimer derivative (**Alexa^b-C5-(BC)$_3$**) of the novel bicyclic ligand **6** mediates predominant delivery to hepatocytes versus nonparenchymal cells (Kupffer, stellate) in vivo. In addition, the hepatic distribution of this representative compound appeared to be perivenous, with the greatest accumulation around the central vein of hepatic lobules.

By all measures, derivatives of bicyclic analogue **6** exhibited superior hepatoselective delivery compared to GalNAc. Quantification of **Alexa^b-C5-(GalNAc)$_3$** and **Alexa^b-C5-(BC)$_3$** liver exposure by multiple methods showed that, upon administration in mice, the trivalent conjugate of **6** facilitated increased ASGPR-directed hepatocellular uptake and prolonged retention compared to the GalNAc conjugate. Lastly, very high liver/plasma ratios were obtained in rats for the delivery of derivatives of the drug RU-486. In particular, we were able to take advantage of this phenomenon to release a passively permeable small-molecule cargo (**RU-furan**) via a triggered cleavable linker (the retro-Diels−Alder release from oxanorbornadienes) to achieve excellent liver/plasma distribution after intravenous infusion. This distribution would be impossible to achieve for the small molecule alone. Pharmacodynamics studies involving such molecular cargo will be explored and described separately. We anticipate that the highly efficient ASGPR-targeting ligands described here, coupled with triggered release and endosomal escape functions when needed, provide an exciting way to reduce dose, modulate the pharmacology of liver targeting, and improve pharmacological selectivity of hepatocytic therapeutics.

■ ASSOCIATED CONTENT

Supporting Information

The Supporting Information is available free of charge on the ACS Publications website at DOI: 10.1021/jacs.6b12964.

Details and additional data concerning small-molecule syntheses, assembly of multivalent conjugates, and studies of binding (surface plasmon resonance), cellular uptake (flow cytometry, fluorescence microscopy, and pulse-chase experiments), serum stability, biodistribution, and molecular structure (X-ray crystallography) (PDF)

CIF file of compound **6** (CIF)

■ AUTHOR INFORMATION

Corresponding Authors

*mgfinn@gatech.edu

*Vincent.Mascitti@pfizer.com

ORCID

M. G. Finn: 0000-0001-8247-3108

Notes

The authors declare the following competing financial interest(s): All authors, except Finn, Sanhueza, Dutta, and Baksh were employed by Pfizer, Inc. at the time this work was done.

■ ACKNOWLEDGMENTS

This work was supported by the Georgia Institute of Technology, The Skaggs Institute for Chemical Biology at The Scripps Research Institute, and Pfizer Global R&D. We thank Dr. Brian Samas (Pfizer) for assistance with the single-crystal X-ray diffraction analysis of compound **12**. All work with animals was approved by the IACUC and was conducted in the Pfizer, Inc., Groton laboratories.

■ REFERENCES

(1) Zelensky, A. N.; Gready, J. E. *FEBS J.* **2005**, *272*, 6179−6217.

(2) Lepenies, B.; Lee, J.; Sonkaria, S. *Adv. Drug Delivery Rev.* **2013**, *65*, 1271−1281.

(3) See ref 4 for citations to various examples.

(4) Stokmaier, D.; Khorev, O.; Cutting, B.; Born, R.; Ricklin, D.; Ernst, T. O. G.; Boni, F.; Schwingruber, K.; Gentner, M.; Wittwer, M.; Spreafico, M.; Vedani, A.; Rabbani, S.; Schwardt, O.; Ernst, B. *Bioorg. Med. Chem.* **2009**, *17*, 7254−7264 and references therein.

(5) Valentijn, A. R. P. M.; van der Marel, G. A.; Sliedregt, L. A. J. M.; van Berkel, T. J. C.; Biessen, E. A. L.; van Boom, J. H. *Tetrahedron* **1997**, *53*, 759−770.

(6) Sliedregt, L. A. J. M.; Rensen, P. C. N.; Rump, E. T.; van Santbrink, P. J.; Bijsterbosch, M. K.; Valentijn, A. R. P. M.; van der Marel, G. A.; van Boom, J. H.; van Berkel, T. J. C.; Biessen, E. A. L. *J. Med. Chem.* **1999**, *42*, 609−618.

(7) Khorev, O.; Stokmaier, D.; Schwardt, O.; Cutting, B.; Ernst, B. *Bioorg. Med. Chem.* **2008**, *16*, 5216−5231.

(8) Lee, R. T.; Lee, Y. C. *Glycoconjugate J.* **2000**, *17*, 543−551.

(9) Pathak, P. O.; Nagarsenker, M. S.; Barhate, C. R.; Padhye, S. G.; Dhawan, V. V.; Bhattacharyya, D.; Viswanathan, C. L.; Steiniger, F.; Fahr, A. *Carbohydr. Res.* **2015**, *408*, 33−43.

(10) Mamidyala, S. K.; Dutta, S.; Chrunyk, B. A.; Préville, C.; Wang, C.; Withka, J. M.; McColl, A.; Subashi, T. A.; Hawrylik, S. J.; Griffor, M. C.; Kim, S.; Pfefferkorn, J. A.; Price, D. A.; Menhaji-Klotz, E.; Mascitti, V.; Finn, M. G. *J. Am. Chem. Soc.* **2012**, *134*, 1978−1981.

(11) Riva, C. Targeting the liver via the asialoglycoprotein-receptor: Synthesis of directed small molecule libraries for the H1-CRD. Ph.D. Thesis, University of Basel, 2006.

(12) Wong, T. C.; Townsend, R. R.; Lee, Y. C. *Carbohydr. Res.* **1987**, *170*, 27−46.

(13) Kolatkar, A. R.; Weis, W. I. *J. Biol. Chem.* **1996**, *271*, 6679−6685.

(14) Rees, D. C.; Congreve, M.; Murray, C. W.; Carr, R. *Nat. Rev. Drug Discovery* **2004**, *3*, 660−672.

(15) Hopkins, A. L.; Groom, C. R.; Alex, A. *Drug Discovery Today* **2004**, *9*, 430−431.

(16) Kuntz, I. D.; Chen, K.; Sharp, K. A.; Kollman, P. A. *Proc. Natl. Acad. Sci. U. S. A.* **1999**, *96*, 9997−10002.

(17) Andrews, P. R.; Craik, D. J.; Martin, J. L. *J. Med. Chem.* **1984**, *27*, 1648−1657.

(18) For a discussion of the influence of van der Waals interactions in the ability of the rat hepatic lectin (RHL1) to bind GalNAc better than Gal, see: Kolatkar, A. R.; Leung, A. K.; Isecke, R.; Brossmer, R.; Drickamer, K.; Weis, W. I. *J. Biol. Chem.* **1998**, *273*, 19502−19508.

(19) Mascitti, V.; Thuma, B. A.; Smith, A. C.; Robinson, R. P.; Brandt, T.; Kalgutkar, A. S.; Maurer, T. S.; Samas, B.; Sharma, R. *MedChemComm* **2013**, *4*, 101−111.

(20) Mascitti, V.; Maurer, T. S.; Robinson, R. P.; Bian, J. W.; Boustany-Kari, C. M.; Brandt, T.; Collman, B. M.; Kalgutkar, A. S.; Klenotic, M. K.; Leininger, M. T.; Lowe, A.; Maguire, R. J.; Masterson, V. M.; Miao, Z.; Mukaiyama, E.; Patel, J. D.; Pettersen, J. C.; Preville, C.; Samas, B.; She, L.; Sobol, Z.; Steppan, C. M.; Stevens, B. D.; Thuma, B. A.; Tugnait, M.; Zeng, D. X.; Zhu, T. *J. Med. Chem.* **2011**, *54*, 2952−2960.

(21) Osuga, D. T.; Feather, M. S.; Shah, M. J.; Feeney, R. E. *J. Protein Chem.* **1989**, *8*, 519−528.

(22) Schaffer, R. *J. Am. Chem. Soc.* **1959**, *81*, 5452−5454.

(23) Smith, E. A.; Thomas, W. D.; Kiessling, L. L.; Corn, R. M. *J. Am. Chem. Soc.* **2003**, *125*, 6140−6148.

DOI: 10.1021/jacs.6b12964
J. Am. Chem. Soc. 2017, 139, 3528−3536

(24) Paulsen, H.; Paal, M. *Carbohydr. Res.* **1984**, *135*, 53−69.
(25) Meier, M.; Bider, M. D.; Malashkevich, V. N.; Spiess, M.; Burkhard, P. *J. Mol. Biol.* **2000**, *300*, 857−865.
(26) The GalNAc binding pocket in the ASGPR receptor has a theoretical maximal binding affinity of 1.3 μM based on a computational druggability assessment. For this method, see: Cheng, A. C.; Coleman, R. G.; Smyth, K. T.; Cao, Q.; Soulard, P.; Caffrey, D. R.; Salzberg, A. C.; Huang, E. S. *Nat. Biotechnol.* **2007**, *25*, 71−75.
(27) Kolatkar, A. R.; Leung, A. K.; Isecke, R.; Brossmer, R.; Drickamer, K.; Weis, W. I. *J. Biol. Chem.* **1998**, *273*, 19502−19508.
(28) Feinberg, H.; Torgersen, D.; Drickamer, K.; Weis, W. I. *J. Biol. Chem.* **2000**, *275*, 35176−35184.
(29) Lodish, H. F. *Trends Biochem. Sci.* **1991**, *16*, 374−377.
(30) Chiu, M. H.; Thomas, V. H.; Stubbs, H. J.; Rice, K. G. *J. Biol. Chem.* **1995**, *270*, 24024−24031.
(31) Kim, E. M.; Jeong, H. J.; Park, I. K.; Cho, C. S.; Moon, H. B.; Yu, D. Y.; Bom, H. S.; Sohn, M. H.; Oh, I. J. *J. Controlled Release* **2005**, *108*, 557−567.
(32) Torres, S.; Martins, J. A.; Andre, J. P.; Neves, M.; Santos, A. C.; Prata, M. I. M.; Geraldes, C. *Radiochim. Acta* **2007**, *95*, 343−349.
(33) Rajeev, K. G.; Nair, J. K.; Jayaraman, M.; Charisse, K.; Taneja, N.; O'Shea, J.; Willoughby, J. L. S.; Yucius, K.; Nguyen, T.; Shulga-Morskaya, S.; Milstein, S.; Liebow, A.; Querbes, W.; Borodovsky, A.; Fitzgerald, K.; Maier, M. A.; Manoharan, M. *ChemBioChem* **2015**, *16*, 903−908.
(34) Nair, J. K.; Willoughby, J. L. S.; Chan, A.; Charisse, K.; Alam, M. R.; Wang, Q.; Hoekstra, M.; Kandasamy, P.; Kel'in, A. V.; Milstein, S.; Taneja, N.; O'Shea, J.; Shaikh, S.; Zhang, L.; van der Sluis, R. J.; Jung, M. E.; Akinc, A.; Hutabarat, R.; Kuchimanchi, S.; Fitzgerald, K.; Zimmermann, T.; van Berkel, T. J. C.; Maier, M. A.; Rajeev, K. G.; Manoharan, M. *J. Am. Chem. Soc.* **2014**, *136*, 16958−16961.
(35) Yu, R. Z.; Graham, M. J.; Post, N.; Riney, S.; Zanardi, T.; Hall, S.; Burkey, J.; Shemesh, C. S.; Prakash, T. P.; Seth, P. P.; Swayze, E. E.; Geary, R. S.; Wang, Y.; Henry, S. *Mol. Ther.–Nucleic Acids* **2016**, *5*, e317.
(36) Link, J. T.; Sorensen, B.; Patel, J.; Grynfarb, M.; Goos-Nilsson, A.; Wang, J. H.; Fung, S.; Wilcox, D.; Zinker, B.; Nguyen, P.; Hickman, B.; Schmidt, J. M.; Swanson, S.; Tian, Z. P.; Reisch, T. J.; Rotert, G.; Du, J.; Lane, B.; von Geldern, T. W.; Jacobson, P. B. *J. Med. Chem.* **2005**, *48*, 5295−5304.
(37) Kislukhin, A. A.; Higginson, C. J.; Hong, V. P.; Finn, M. G. *J. Am. Chem. Soc.* **2012**, *134*, 6491−6497.
(38) Hong, V.; Kislukhin, A.; Finn, M. G. *J. Am. Chem. Soc.* **2009**, *131*, 9986−9994.
(39) Hudgin, R. L.; Pricer, W. E. J.; Ashwell, G.; Stockert, R. J.; Morell, A. G. *J. Biol. Chem.* **1974**, *249*, 5536−5543.
(40) Ashwell, G.; Morell, A. G. *Adv. Enzymol. Relat. Areas Mol. Biol.* **1974**, *41*, 99−128.
(41) Vercauteren, D.; Vandenbroucke, R. E.; Jones, A. T.; Rejman, J.; Demeester, J.; De Smedt, S. C.; Sanders, N. N.; Braeckmans, K. *Mol. Ther.* **2010**, *18*, 561−569.
(42) D'Souza, A. A.; Devarajan, P. V. *J. Controlled Release* **2015**, *203*, 126−139.
(43) Weigel, P. H.; Yik, J. H. N. *Biochim. Biophys. Acta, Gen. Subj.* **2002**, *1572*, 341−363.
(44) Schwartz, A. L.; Fridovich, S. E.; Lodish, H. F. *J. Biol. Chem.* **1982**, *257*, 4230−4237.
(45) This compound was administered in a formulation of DMSO/PEG-400/12.5% SBE−cyclodextrin in water (1/10/89 v/v). The mixture was filtered prior to dosing to avoid the injection of undissolved compound; analysis of three 20 μL aliquots established the measured dose as 1.5 mg/kg.
(46) Higginson, C. J.; Eno, M. R.; Khan, S.; Cameron, M. D.; Finn, M. G. *ACS Chem. Biol.* **2016**, *11*, 2320−2327.
(47) Shemesh, C. S.; Yu, R. Z.; Gaus, H. J.; Greenlee, S.; Post, N.; Schmidt, K.; Migawa, M. T.; Seth, P. P.; Zanardi, T. A.; Prakash, T. P.; Swayze, E. E.; Henry, S. P.; Wang, Y. *Mol. Ther.–Nucleic Acids* **2016**, *5*, e319.
(48) Voorschuur, A. H.; Kuiper, J.; Neelissen, J. A. M.; Boers, W.; Van Berkel, T. J. C. *Biochem. J.* **1994**, *303*, 809−816.
(49) Griffith, L. G.; Lopina, S. *Biomaterials* **1998**, *19*, 979−986.
(50) Lai, C. H.; Lin, C. Y.; Wu, H. T.; Chan, H. S.; Chuang, Y. J.; Chen, C. T.; Lin, C. C. *Adv. Funct. Mater.* **2010**, *20*, 3948−3958.
(51) Yang, Y. S.; Thomas, V. H.; Man, S. C.; Rice, K. G. *Glycobiology* **2000**, *10*, 1341−1345.
(52) Prata, M. I. M.; Santos, A. C.; Torres, S.; Andre, J. P.; Martins, J. A.; Neves, M.; Garcia-Martin, M. L.; Rodrigues, T. B.; Lopez-Larrubia, P.; Cerdan, S.; Geraldes, C. *Contrast Media Mol. Imaging* **2006**, *1*, 246−258.
(53) Matsuda, S.; Keiser, K.; Nair, J. K.; Charisse, K.; Manoharan, R. M.; Kretschmer, P.; Peng, C. G.; Kel'in, A. V.; Kandasamy, P.; Willoughby, J. L. S.; Liebow, A.; Querbes, W.; Yucius, K.; Nguyen, T.; Milstein, S.; Maier, M. A.; Rajeev, K. G.; Manoharan, M. *ACS Chem. Biol.* **2015**, *10*, 1181−1187.
(54) David, A.; Kopeckova, P.; Minko, T.; Rubinstein, A.; Kopecek, J. *Eur. J. Cancer* **2004**, *40*, 148−157.
(55) Gomez-Valades, A. G.; Molas, M.; Vidal-Alabro, A.; Bermudez, J.; Bartrons, R.; Perales, J. C. *J. Controlled Release* **2005**, *102*, 277−291.
(56) Rozema, D. B.; Lewis, D. L.; Wakefield, D. H.; Wong, S. C.; Klein, J. J.; Roesch, P. L.; Bertin, S. L.; Reppen, T. W.; Chu, Q.; Blokhin, A. V.; Hagstrom, J. E.; Wolff, J. A. *Proc. Natl. Acad. Sci. U. S. A.* **2007**, *104*, 12982−12987.
(57) Biessen, E. A. L.; Bakkeren, H. F.; Beuting, D. M.; Kuiper, J.; Van Berkel, T. J. C. *Biochem. J.* **1994**, *299*, 291−296.

DOI: 10.1021/jacs.6b12964
J. Am. Chem. Soc. 2017, 139, 3528−3536